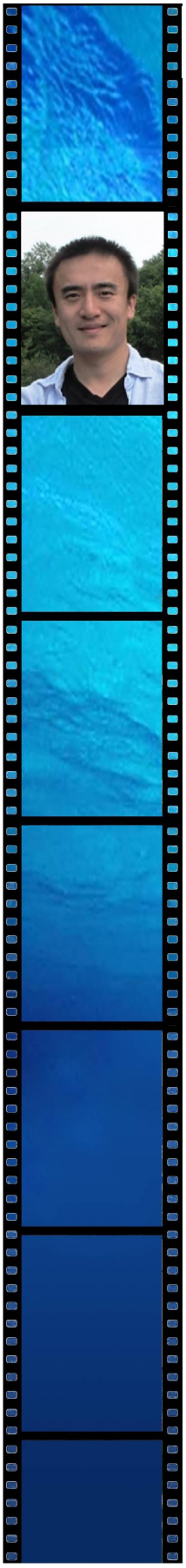

Article

MAPPING MESOSCALE OCEAN CURRENTS

By Dr. L. Zhou (USA)
Graduate School of Oceanography, University of Rhode Island
South Ferry Road, Narragansett, RI 02882

Abstract

This paper presents the technical aspects, error analysis and result comparison of a flexible mapping method particularly useful in regional ocean studies. Mesoscale ocean currents are computed from multiple satellite altimeter along-track measurements via objective analysis with a data-derived space-time correlation model. The additional satellite tracks help resolve more eddies with smaller radii and reduce the overall domain-wide mapping errors. The mapping results are consistent with the *in-situ* hydrographic data and Lagrangian data from a surface drifting buoy. The mapped currents have optimal spatial and temporal resolutions that can benefit the studies of mesoscale variability and surface particle dispersion simulation.

Résumé

Cet article présente les aspects techniques, l'analyse d'erreurs et la comparaison des résultats d'une méthode flexible de cartographie particulièrement utile dans le cadre des études océaniques régionales. Les courants océaniques à méso-échelle sont calculés à partir de multiples mesures longitudinales par satellite altimétrique *via* une analyse objective avec un modèle de corrélation espace-temps issu des données. Les routes additionnelles du satellite aident à résoudre de plus nombreux tourbillons avec moins de *radii* et à réduire les erreurs d'ensemble d'un vaste domaine cartographique. Les résultats cartographiques sont compatibles avec les données hydrographiques *in-situ* et les données de Lagrange à partir d'une bouée de surface dérivante. Les courants représentés ont des résolutions spatiales et temporelles optimums qui peuvent améliorer les études de variabilité à méso-échelle et la simulation de la dispersion des particules en surface.

Resumen

Este artículo presenta los aspectos técnicos, el análisis de errores y la comparación de los resultados de un método cartográfico flexible particularmente útil en los estudios de los océanos regionales. Las corrientes oceánicas a media distancia se calculan a partir de medidas de pistas longitudinales efectuadas por altímetro de acceso a satélites múltiples mediante un análisis objetivo con un modelo de correlación espacio-tiempo derivado de los datos. Las pistas adicionales del satélite ayudan a resolver más remolinos con radios menores y a reducir los errores generales de cartografía en todos los campos. Los resultados cartográficos son coherentes con los datos hidrográficos *in-situ* y con los datos lagrangianos procedentes de una boya libre de superficie. Las corrientes representadas tienen resoluciones espaciales y temporales óptimas que pueden ser beneficiosas para los estudios de variabilidad a media distancia y para la simulación de dispersión de partículas de superficie.

1. Introduction

The study of mesoscale variability of currents in space and time relies on constructing snapshots of flow field from measurements that are not sampled uniformly. Mapping mesoscale ocean currents is also the basis for the simulation of turbulent eddy stirring where numerical drifters are deployed and dispersed by the mapped currents varying with time (Zhou et al., 2009). Mesoscale eddies (spatial scale between 30 to 1000 km), the most energetic component of the ocean, play an important role in modifying the local hydrographic structure and circulation by transporting momentum and tremendous kinetic energy. Beyond the field of Physical Oceanography, mapping of mesoscale currents on desired grids is of general value and is useful in various applications such as search and rescue operations, pollution transport and fishing activities.

How well the mapping process can resolve mesoscale eddies is important and depends on a number of factors including the original sampled measurements, correlations among these measurements and mapping grid resolutions. In this paper we discuss the objective mapping of multiple along-track satellite altimeter measurements, which uses a data-derived space-time correlation model with optimum spatial mapping resolution specifically for the area of interest. Our study area is identical to the domain of Lagrangian Isopycnal Dispersion Experiment (LIDEX), in which 10 clusters of isopycnal RAFOS floats were deployed at two depths south of the Cape Verde Islands in the tropical North Atlantic in April 2003 to investigate the isopycnal dispersion by mesoscale eddies (***Figure 1***).

Many studies (Ducet et al., 2000) have shown that the sea level anomalies (SLA) can be measured with satellite altimeters by applying various corrections and removing the mean sea surface height. Objective analysis of along-track altimeter measurements allows data with different spatial and temporal resolutions to generate SLA maps with uniform temporal and spatial resolution. Surface velocities then can be derived from these SLA maps by assuming the flow is geostrophic if the Rossby Number is small:

$$R_o = \frac{U}{fL} \quad , \qquad (1)$$

where U and L are, respectively, the characteristic velocity and length scales of the phenomenon. The Coriolis frequency is $f = 2\Omega \sin\varphi$ at latitude, φ and Ω is the angular velocity of planetary rotation.

Then the geostrophic velocities can be estimated as follows:

$$u = -\frac{g}{f}\frac{\partial \eta}{\partial y} \quad , \quad v = \frac{g}{f}\frac{\partial \eta}{\partial x} \qquad (2)$$

where u and v are the velocity component along zonal direction i and meridional direction j respectively, η is the SLA and g is the gravitational acceleration. Zonal and meridional velocities were determined by finite difference of the daily SLA field:

$$u_{(i,j)} = -\frac{g_{(i,j)}}{f_{(i,j)}}\left(\frac{\eta_{(i+1,j)} - \eta_{(i-1,j)}}{2\Delta y}\right), v_{(i,j)} = \frac{g_{(i,j)}}{f_{(i,j)}}\left(\frac{\eta_{(i,j+1)} - \eta_{(i,j-1)}}{2\Delta x}\right) \qquad (3)$$

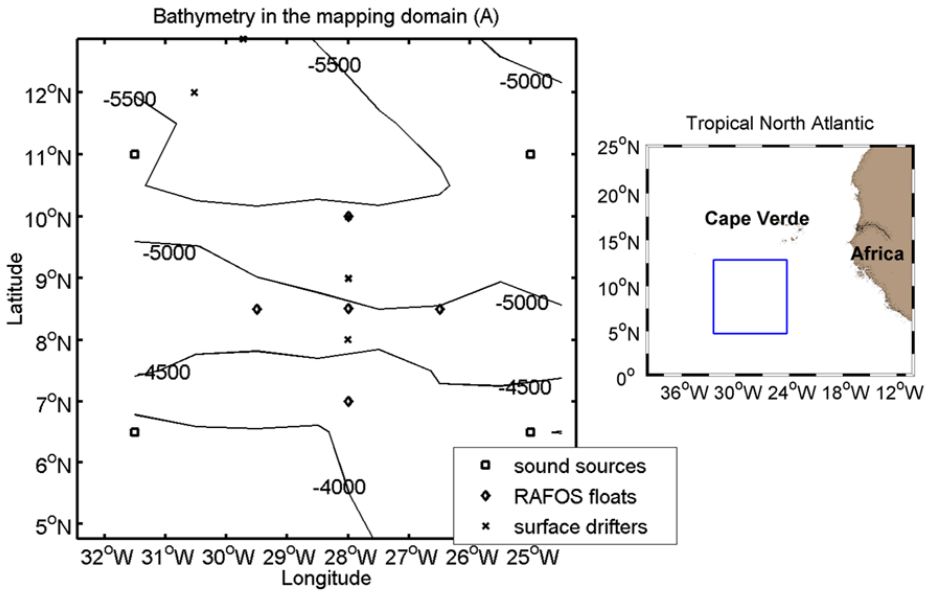

Figure 1*: Objective mapping domain chosen to coincide with the Lagrangian Isopycnal Dispersion Experiment (LIDEX) site in the center. On the left panel, squares indicate the locations of four sound sources, diamonds show where the floats were deployed and crosses are the deployment of surface drifters. The bathymetry contours are in metres (Source: Smith & Sandwell 2-minute gridded ocean bathymetry).*

The theory above enables mesoscale currents to be determined from SLA maps. It is important to note the mesoscale current is a major part of the overall flow field, which additionally includes the temporally mean currents, the wind driven Ekman flow[1], and the sub-mesoscale flow that is not observed by altimeters but may dominate short-term dispersion.

In this paper we focus on the technical aspects of objective mapping of sea level. In Section 2, we introduce five along-track altimeter data sets that are used in this study. In Section 3, we construct a space-time correlation model from all available SLA data based on their ensemble average spatial and temporal correlation functions. In Section 4, we analyze the mapping errors of objective analysis and present an example of mapped mesoscale flow field to discuss the effects of along-track measurements in different resolutions. In Section 5, the mapped results are compared with in-situ hydrographic data and trajectory of a drifting buoy. Section 6 is a summary of major findings and possible advantages of this mapping method in local or regional studies.

2. Data

The sea level anomalies (SLA) can be derived by subtracting the geoid height from the variable sea surface height. In reality the geoid is difficult to determine accurately, so a mean sea level over 7 years is subtracted instead. Along-track SLA data of five altimeters were obtained from Global Near-real-time Sea Surface Anomaly Data server at Colorado Center for Astrodynamics Research (CCAR).

In this study our objective analysis employs along-track SLA data from available operating altimeters during three years from 2003 to 2006, namely Topex/Poseidon, Jason-1, ERS-2, Envisat, and Geosat Follow-on (GFO). Table 1 shows a breakdown of the available time frames for these altimeters during our time of study. Topex/Poseidon and Jason-1 follow a repeat cycle of ten days designed to monitor ocean variations, so they pass over the same points every 10 days but their ground tracks are approximately 315 kilometers apart at the equator. On September 15, 2002 Topex/Poseidon assumed a new orbit midway between its original ground tracks. The former Topex/Poseidon ground tracks are overflown by Jason-1. This essentially doubles the data resolution. On the other hand, ERS-2 and Envisat only revisit the same point on the globe every 35 days but the maximum distance between two tracks at the equator is just 80 kilometers. GFO (Geosat Follow-on) follows the 17-day repeat orbit of Geosat whose primary task was to measure the marine geoid, and contributes additional survey points to our along-track dataset.

All five SLA datasets have been processed for corrections. First of all the data are corrected for instrument errors and environmental effects. Then geophysical corrections are applied, including solid earth, water vapor, waves and tides, and the pole tide. The validation process done by the CCAR provided preliminary quality controls to reduce systematic errors. The following additional steps prepare the data for the objective analysis in order to eliminate singular values and to minimize mapping errors. Given that the average SLA magnitude is 40 mm with a standard deviation of 50 mm over the three years, the SLA values that are greater than 700 mm and differ from neighboring points along the same track by 100 mm are regarded as singular points and excluded. Less than 1% of the data were removed after this procedure. The grid resolution of objective analysis should be comparable to the average along-track resolution of all altimeters, and at least two times smaller than the diameter of the smallest eddies to be resolved. The chosen resolution is 9 km based on these criteria :

3. Space-Time Correlation Model

Objective analysis (OA) uses statistical knowledge of mesoscale currents variability as expressed in covariance functions of the signal and associated noise, and then allows the data to be projected onto grid locations with uncertainty estimates. This technique deals with data with irregular gaps both in space and time. The construction of the correlation model functions is of major importance to this method. When there are sufficient data present, the correlations are calculated from the quantities in terms of spatial and temporal lags. A space-time correlation model is determined based on the correlation curves and applicable to data within the correlation scales. This way it treats space and time in an associated way so that the value at a certain space and time is related with the data measured at different locations and times. In constructing the correlation functions, it is assumed that the generated mesoscale flow field is time-dependent but statistically stationary and spatially isotropic. Although the mesoscale field may not be isotropic in the real ocean, it is still assumed isotropic in our analysis because we don't intend to presume how anisotropic the mesoscale features actually are. If the final statistics are nevertheless anisotropic, then this result is more robust.

Within the square 900 × 900 km domain (***Figure 1***), the spatial autocorrelation function is derived from along-track SLA measurements along all satellite ground tracks. The along-track measurements have different spatial resolutions among altimeters. Therefore all the autocorrelation functions are determined separately and then binned onto 6.39 km grids, which is the average value of altimeter resolutions. The fitted curve is generated based on the ensemble average of all autocorrelation functions ***(Figure 3)*** which is defined by:

$$C(r) = \exp(-\frac{r}{90})\cos(\frac{2\pi r}{920}) \qquad (4)$$

where along-track distance $r = \sqrt{\Delta x^2 + \Delta y^2}$, Δx and Δy being the zonal and meridional lags, respectively. A curve is fitted to the entire curve of the average correlation curve ***(Figure 3)***.

1: Wind driven currents flowing at an angle to the driving winds.

For the objective maps, SLA measurements within an OA search radius of 187 km in space, the zero crossing with x-axis of the average autocorrelation, of each grid point are used. The spatial scale of search radius is close to the average deformation radius, which defines theoretically the radius of mesoscale coherent eddies. Within the search radius, the dominant term in Equation (4) is the exponential term and the cosine term does not change the fitted curve significantly.

The temporal correlation function is estimated from Topex/Poseidon and Jason-1 instead of all altimeters, because Topex/Poseidon and Jason-1 have the shortest repeat cycle 10 days or the highest data sampling frequency. All time series of 300 days long during 3 years at 40 locations throughout the domain are used for calculating the ensemble average of temporal correlation. The zero crossing 52 days defines the OA search range in time (lower panel, ***Figure 2***). The fitted curve models how fast the SLA at one location becomes uncorrelated within the OA temporal search range both before and after the target time. The temporal correlation function is dependent on time lag Δt in days and exponentially decreases:

$$C(\Delta t) = \exp(-\frac{|\Delta t|}{32}) \qquad (5)$$

Satellite	Topex/ Poseidon	Jason-1	ERS-2	Envisat	GFO (Geosat Follow-on)
Available time frame	2/5/03 to 10/1/05	2/5/03 to 3/20/06	2/5/03 to 6/7/05	2/5/03 to 3/20/06	2/5/03 to 3/20/06

Table 1*: The time line of each altimeter from 2/5/03 to 3/20/06 in this study.*

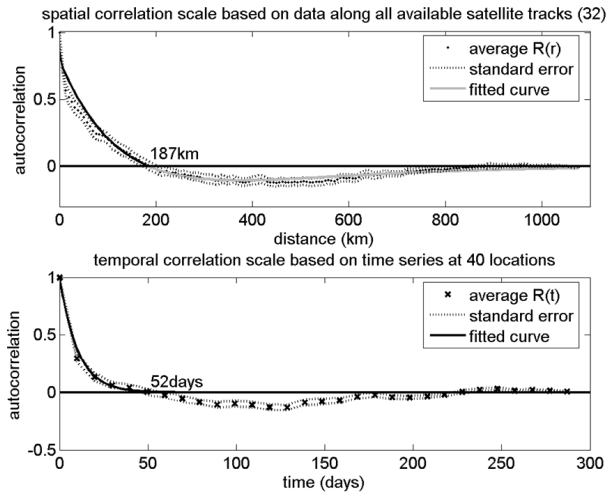

Figure 2: *Spatial correlation (upper) based on measured SLA along all satellite ground tracks and temporal correlation (lower) based on 40 SLA time series during 2 years from Jason-1 and Topex/ Poseidon for domain A. Dotted lines are the standard errors with 95% confidence level. The OA search radius 187 km and 52 days are respectively the zero crossings with x-axis of the average correlation curves. Fitted curves are based on the average correlation within the search radius.*

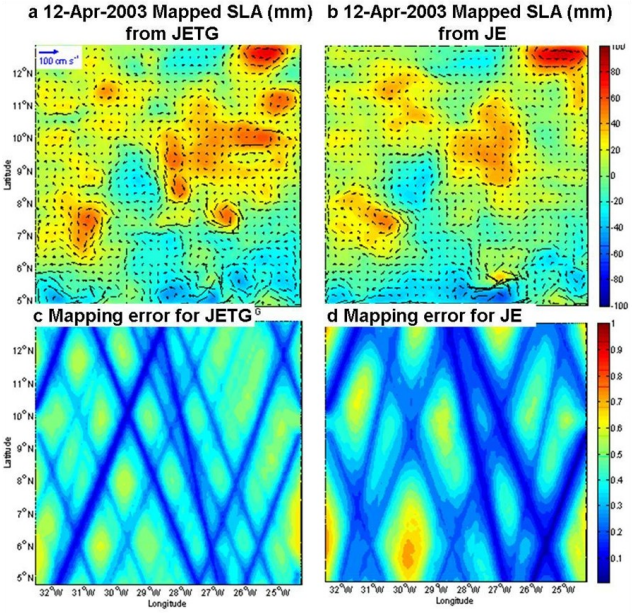

Figure 3*: One example of mapped mesoscale flow field on 4/12/2003. Panel (a) and (b) are the mapped SLA with superimposed geostrophic velocity vectors based on four satellites (JETG: Jason-1, Envisat, T/P, GFO) and two satellites (JE: Jason-1, Envisat), respectively. In panel (a) and (b), warm-colored eddies are positive SLA or clockwise swirling eddies and vise versa for cold-colored ones. Additional eddies with small radii can be resolved with the combination of two extra altimeters. Panel (c) and (d) shows the associated mapping uncertainty as a fraction of data variance. The overall errors are lower in Panel (c) with more SLA data available.*

In the tropical eastern North Atlantic ocean, mesoscale eddies migrate generally westward (Cushman-Roisin et al., 1990). The spatial correlation changes in time as eddies move through satellite ground tracks. However, it is a reasonably good estimate of the de-correlation time given that the temporal correlation is based on many time series at locations spaced differently across the study area. This statistical propagation tendency needs to be accounted for in the OA space-time correlation model (e.g., McGillicuddy et al., 2001; Thiebaux and Pedder, 1987). This is achieved by changing the radial coordinate r at each time step to reflect the effects of westward phase propagation (Siegel et al., 1999):

$$R = \sqrt{(\Delta x - c\Delta t)^2 + \Delta y^2} \qquad (6)$$

where R is the new radial coordinate at the next time step in km. The phase speed c of westward migration is 4.5 cm/s, which is derived by tracking APEX floats and comparing satellite images in six months after September 2000 (Stramma et al., 2005), and close to the result from in situ measurement in the eastern North Atlantic by Pingree (2002). The phase speed correction does not change the total area within the search radius at each time step but its distribution around the grid point. The data would be gathered from up to 230 km west of the grid point at times up to 52 days before the current time.

The spatial correlation function determined earlier is not affected by this advective effect. To test this, SLA values are derived with interpolation at new tracks that shift westward from the original 32 tracks to account for the phase speed correction. The new correlation curve is very similar to the original one with a root-mean-square difference of 0.03. Therefore the final space-time correlation model used in the objective mapping is:

$$C(R,\Delta t) = \exp(-\frac{R}{90})\cos(\frac{2\pi R}{920})\exp(-\frac{|\Delta t|}{32}) \qquad (7)$$

4. Objective Analysis and Mapping Errors

Based on this space-time correlation model, the objective analysis is a statistical technique to determine the best linear unbiased estimate for a location where there is no altimeter measurement. Daily SLA maps are generated with spatial resolution of 9 km during 2/25/2003-2/25/2006 from multiple altimeters. In this section we will introduce the theory of objective analysis and address mapping errors. Consider at a certain time, the SLA value is not available at the *i*th grid point where there is no altimeter measurement. An estimate of the true value η_i can be based on all available measurements within a spatial radius. The estimated value $\hat{\eta}_i$ is the sum of a set of weights w_k multiplied by the measurements η_k, as follows:

$$\hat{\eta}_i = \sum_k w_k \eta_k \qquad (8)$$

The expected error in this estimate is quantified as the error variance $\hat{e}_i^2$:

$$\hat{e}_i^2 = \left\langle \left[\eta_i - \sum_k w_k \eta_k \right]^2 \right\rangle = \langle \eta_i \eta_i \rangle - 2\sum_k w_k \langle \eta_i \eta_k \rangle + \sum_k \sum_m w_k w_m \langle \eta_k \eta_m \rangle \qquad (9)$$

where the bracket $\langle\ \rangle$ represents the expectation value.

The purpose of objective analysis is to find weights and the error variance $\hat{e}_i^2$. The unknown weights can be w_k solved by minimizing the expected error in Equation (9), which is expressed as:

$$\partial \hat{e}_i^2 / \partial w_k = 0 \qquad (10)$$

From Equation (9) and (10), we have:

$$\sum_m w_m \langle \eta_k \eta_m \rangle = \langle \eta_k \eta_i \rangle, k = 1,2,...,N \qquad (11)$$

The true SLA value η_i is unknown. The expectation terms are equal to covariances that can be estimated with the correlation model function statistically determined earlier:

$$\langle \eta_k \eta_i \rangle = C(R_{ki}, 0) \qquad (12)$$

where R_{ki} is the separation distance between the *k*th and *i*th grid points. Adding the temporal dimension of the correlation model, Equation (12) combines the available measurements within the temporal search radius by taking the form of $C(0,\Delta t_{ki})$.

In a matrix form, Equation (11) is converted to:

$$C_{km} W = C_{ki} \qquad (13)$$

C_{km} is the $N \times N$ data covariance matrix, and C_{ki} is the $N \times 1$ estimate-data covariance vector. W is $N \times 1$ the weight vector. The solution is:

$$W = (C_{km}^{-1} C_{ki})' \text{ , and } \hat{\eta}_i = (C_{km}^{-1} C_{ki})' \eta_k \qquad (14)$$

Larger weights are assigned to the SLA measurements at locations closer to the grid point of interest both in space and time within the search radii, where the correlation value is positive. The expected error variance or confidence level is:

$$\hat{e}_i^2 = C(0,0) - (C_{km}^{-1} C_{ki})' C_{ki} \qquad (15)$$

The first term in Equation (15) represents the expected error that is equivalent to the data covariance as it approaches zero lag in space and time, if there is no data available for the estimation. In this case, the mapping error variance is 1, the same as the measurement error variance, and the estimation is no better than picking any value measured along any satellite ground track. The second term reduces the estimated error because of the new information provided by SLA measurements at grid points in space and time within the search radii of objective analysis. The mapping error variance would be less than 1 and the confidence level of using this estimation is higher than that of picking a random value. Then $\hat{e}_i^2$ in Equation (15) becomes effectively the fraction of mapping error variance relative to the variance of the data. Measurements close in space and time have higher influence on the estimated value. A dense distribution of along-track SLA measurements favors a more accurate estimation of the SLA field.

The averaged SLA over the period of three years is removed at each grid point every day. In the calculation of geostrophic velocities, the noise in the SLA data would likely introduce an erratic and unrealistic component to the eddy flow field. Therefore, every SLA map is smoothed additionally with a rotationally symmetric Gaussian lowpass filter (radius 35 to 65 km). The residual, absolute difference between the original output and the smoothed SLA field, averaged across the domain during three years is 0.4 mm, 0.8% of the ensemble average SLA. As a result, the filtering process does not heavily weaken the overall signal strength. One necessary thing to point out is that although the absolute value of the residue is rather small, at locations where eddies are present the filtering process tends to underestimate the SLA gradient and velocities, especially at lower latitudes where small Coriolis parameter f makes the geostrophic velocities more sensitive to SLA gradient.

One example of mapped SLA field illustrates how the mapping errors can be reduced by combining two more satellites (*Figure 3*). Based on the Equation (15), the mapping error matrix quantifies the level of uncertainties as percentage of the objective mapping error variance relative to the variance of the measurements. A value of 1 suggests that the mapped result is no better than picking a random number from all SLA measurements across the domain, when there is no available data to estimate from. In most occasions, the mapping error variance is less than 1. Panel (a) employs along-track data from four satellites available (JETG: Jason-1, Envisat, T/P, GFO), two more than what panel (b) is based upon (JE: Jason-1, Envisat). The addition of SLA measurements along new ground tracks has provided advantages of resolving more eddies with smaller radii (e.g., eddies at 11°N, 25°W and 7.5°N, 26.5°W) and reducing the overall mapping uncertainty in the domain. The second advantage is clearly seen from the level of uncertainties in Panel (c) and (d). It is evident that the mapping errors increase with the distance away from satellite ground tracks. Panel (c) has relatively lower mapping errors over the domain compared with Panel (d). The addition of new ground tracks reduces the mapping error variance to below 65% of the data variance. The spatially-averaged mapping error variance is calculated to be 40%, or 6 mm across the domain.

5. Comparison of Mapping Results with *in-situ* Data

Maps of mesoscale flow field from the objective analysis are compared to the in-situ hydrographic data and a Lagrangian drifter trajectory. To determine the hydrographic structure around the float deployment locations, a hydrographic survey cruise as part of LIDEX was carried out during 25 days from 3/25/03 to 4/16/03 (*Figure 4*). The high resolution survey consists of CTD (An oceanographic tool to measure Conductivity, Temperature and Depth of sea water) casts spaced every 50 km.

The mapped mesoscale flow field has sufficiently high resolution to provide an effective comparison with the geopotential height anomaly (GPHA) field from LIDEX CTD casts. First, the geopotential height $\Delta\Phi$ is calculated in reference to 1000 db at each station of CTD casts as follows,

$$\Delta\Phi = \int_0^{1000} \delta \cdot dP \,, \qquad (16)$$

where δ represents the specific volume anomaly. $\Delta\Phi$ ranges from -24.1 to 27.9 mm within the surveyed domain. Then after removing the domain-wide average to better show the anomaly size, the GPHA map is generated with linear interpolation onto equal spatial grid, providing surface signatures of what appears to be four eddies.

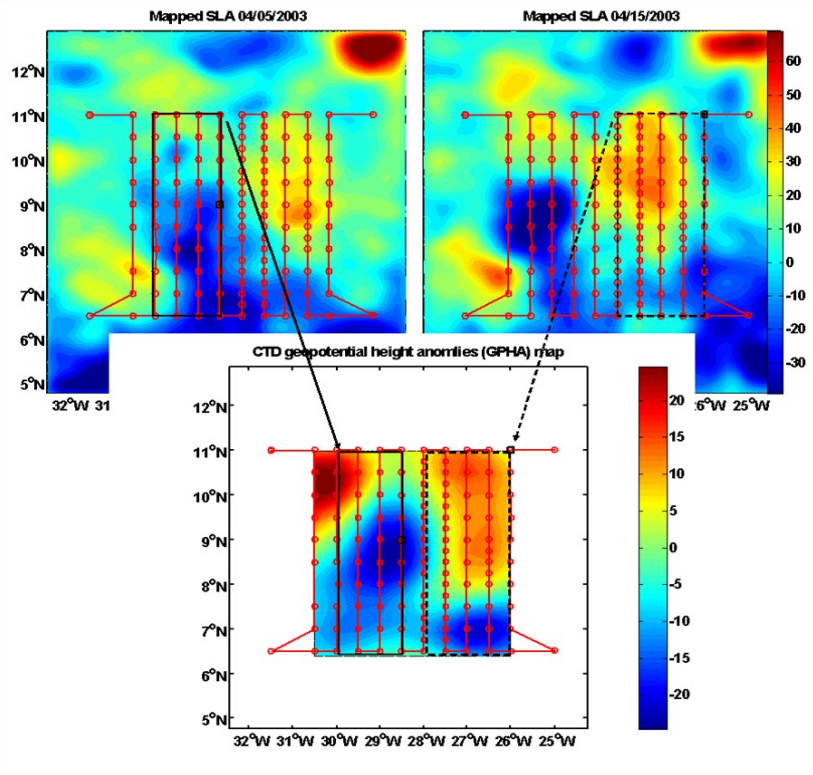

Figure 4: Comparison between mapped SLA fields (upper) and GPHA (geopotential height anomaly) map (lower) from LIDEX hydrographic survey. Red line and circles show the cruise track and stations of CTD casts. Two black squares in the upper 2 panels represent casts taken on 4/5/03 and 4/15/03. Similar eddy distributions can be captured by comparing the areas in black boxes to the left and black dashed boxes to the right. Scales are slightly different because different reference levels are chosen.

The mesoscale flow field was constantly evolving while the CTD data were being collected. If we compare the GPHA map (bottom panel, Figure 4) with the mapped SLA field on 4/5/03 (top panel, Figure 4) and focus upon the area within the black box in each panel, it is found the sea level trends are generally similar, especially along meridional direction. The spatial resemblance is even more prominent between the SLA on 4/15/03 and the GPHA in the area 250 km west of that survey line along 26°W. Nevertheless the scales are slightly different due to the different choices of reference level for SLA and GPHA, which are the statistical mean surface over the period of 1993 to 1999 and the level of no motion (in this case 1000 db), respectively.

The comparison is quantified with correlation between mapped SLA field and CTD data, and between the CTD data and the merged map products distributed by AVISO (Archiving, Validation, and Interpretation of Satellite Oceanographic Data that distributes satellite products). At 123 stations where a CTD cast was taken during 3/26/03 to 4/17/03, the SLA value is estimated by interpolating mapped SLA in space and time.

The correlation coefficient between the mapped SLA and GPHA is 0.47 after the spatial average is removed for both datasets. The same steps are repeated for 5 merged AVISO maps derived from an identical set of satellites during 35 days. The correlation coefficient between the AVISO maps and GPHA is 0.4. As a result, the regional fine-tuning of the correlation model would moderately improve the mapping results.

A SVP (Surface Velocity Program) drifter was deployed on 3/9/2004 and carried towards southwest in a slowly migrating eddy during four months from 3/19/2004 to 6/22/2004. The looping trajectory shows five clockwise circles that are approximately 15 days apart. This indicates that the drifter was entrained in an anti-cyclonic eddy. Five snapshots of mapped SLA field are chosen at the same time as the drifter went through each of the circles. The mapped SLA field correctly reveals an anti-cyclonic eddy migrating towards southwest. In each pair of connected boxes, the looping direction of the drifter agrees with the direction of geostrophic current (***Figure 5***).

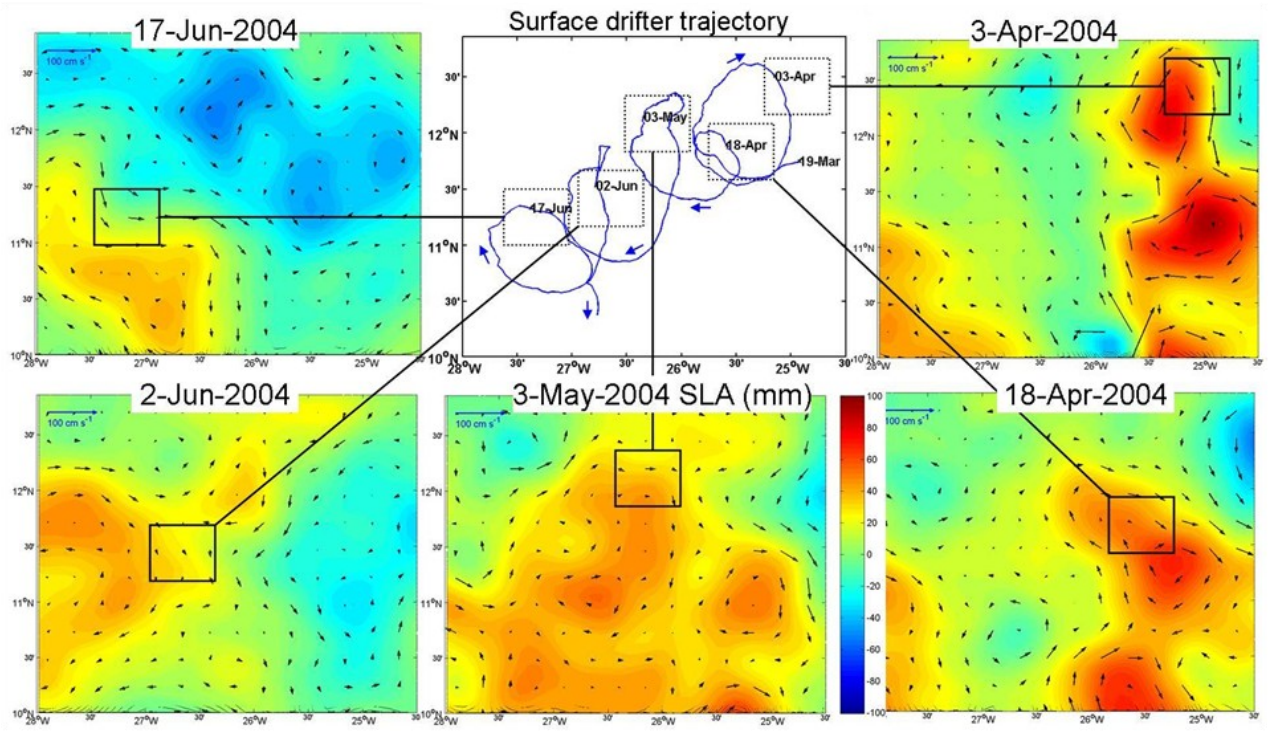

***Figure 5**: Comparison between surface drifter trajectory (center, upper) and mapped SLA field on corresponding dates. The SVP drifter number 44822 (NOAA, The Global Drifter Program) was deployed on 3/9/2004 and caught in an anti-cyclonic eddy moving towards southwest during the period of 3/19 to 6/22/2004. Five snapshots of mapped SLA field show the migration of the same eddy and associated velocity vectors. Similar moving direction can be found by comparing the trajectory and the velocity vectors in each of the five pairs of connected boxes.*

6. Conclusions

The method of mapping ocean currents discussed in this paper has the flexibility to select certain along-track datasets to be used, to optimize mapping grid resolutions, and to further process the data before and after the objective mapping. This mapping method is suitable for regional studies in a certain time frame because the space-time correlation model for objective analysis is constructed directly from the statistics of data within the study area.

For the purposes of investigating mesoscale ocean variability and simulating surface particle dispersion in local or regional scales, the SLA mapping products from the OA procedures have three advantages over AVISO merged maps:

a. The objective mapping with optimized spatial and temporal resolutions can provide data of SLA and velocities on desired grids with error analysis for kinematic models in a specific study area (Zhou et al., 2009).

b. A space-time correlation model with data-derived parameters has been tuned specifically for the study area.

c. Additional quality control or special processing can be done with the original along-track data prior to the objective mapping.

The procedures of objective mapping are tested with different numbers of original along-track altimeter data sets. It is shown that adding SLA measurements along additional ground tracks has provided improvements of resolving more eddies with smaller radii and reducing the overall mapping errors in the domain. A higher resolution of original measurements translates to finer optimum mapping resolution and lower mapping errors in the mapped SLA field. The results of objective analysis are consistent with the hydrographic data during LIDEX cruise and the trajectory of a surface drifter in the northern part of study area. The method is applicable to the mapping of other types of data including sea surface temperature from along-track scanning radiometer measurements.

Acknowledgements

The author would like to thank Dr. David Hebert and Dr. Thomas Rossby for their guidance and advice in his dissertation study. The author also thankfully acknowledges Dr. Valery Kosnyrev and Dr. Dennis McGillicuddy for their assistance and advice with the methodology. The author thanks three anonymous reviewers for their thoughtful inputs and comments that are vital to improving this manuscript. This research was supported by the National Science Foundation under award 0117660 and 0411804. Real-time Altimeter Data Research Group at Colorado Center for Astrodynamics Research (CCAR) is acknowledged for providing the data.

References

Cushman-Roisin, B., E. P. Chassignet, and B. Tang (1990): Westward motion of mesoscale eddies. *J. Phys. Oceanogr.,* **20,** 758–768.

Ducet, N., P.-Y. Le Traon, and G. Reverdin (2000): Global high-resolution mapping of ocean circulation from TOPEX/Poseidon and ERS-1 and -2. *J. Geophys. Res.*, **105**, 19,477-19,498.

McGillicuddy, D. J., Jr., and V. K. Kosnyrev (2001), Dynamical interpolation of mesoscale flows in the TOPEX/Poseidon diamond surrounding the U.S. Joint Global Ocean Flux Study Bermuda Atlantic Time-series Study site, *J. Geophys. Res.*, **106**(C8), 16,641–16,656.

Pingree, R. (2002). Ocean structure and climate (eastern North Atlantic): In situ measurement and remote sensing. *Journal of the Marine Biological Association of the United Kingdom*, **82**(2), 681-707

Siegel, D. A., D. J. McGillicuddy, Jr. and E. A. Fields (1999): Mesoscale eddies, satellite altimetry, and new production in the Sargasso Sea. *J. Geophys. Res.*, **104** (C6), 13359–13379.

Smith, W. H. F., and D. T. Sandwell (1997): Global seafloor topography from satellite altimetry and ship depth soundings. *Science*, **277**, 1957-1962

Stramma, L., S. Huttl, and J. Schafstal (2005): Water masses and currents in the upper tropical northeast Atlantic off northwest Africa. *J.Geophs. Res.*, **110**, C12006

Thiebaux, H. J., and M. A. Pedder (1987): *Spatial Objective Analysis.* Academic Press, 299 pp

Zhou, L. (2009): *Mesoscale Variability and Lagrangian Statistics in the Tropical North Atlantic*, Ph.D. thesis, University of Rhode Island, Graduate School of Oceanography, 110 pp

Biography of the Author

Originally from China, **Long Zhou** received his PhD in Physical Oceanography and MA in Marine Affairs from the University of Rhode Island in 2009. Long's research experience includes studying turbulent dispersion, mapping ocean currents and numerical simulation of pollutant transport. He takes special interest in marine resource management. Besides hands-on research, Long Zhou worked as a policy analyst, an energy consultant and a lab manager since 2003. Since February 2010, Long has been working on the National Ocean Policy and research program analysis in the US National Oceanic and Atmospheric Administration (NOAA).